Computational and Theoretical Methods to Explore the Relation between Enzyme Dynamics and Catalysis

Dimitri Antoniou, Jodi Basner,† Sara Núñez,‡ and Steven D. Schwartz*

Department of Biophysics, Albert Einstein College of Medicine, Yeshiva University, Bronx, New York

Received November 3, 2005

Contents

* Corresponding author. E-mail: sschwartz@aecom.yu.edu.
† Current address: Department of Chemistry and Biochemistry, University of Maryland, College Park, MD.
‡ Current address: Department of Chemical Design and Synthesis, Solvay Pharmaceuticals, The Netherlands.

1. Introduction

The first conference focusing exclusively on the relation between enzyme dynamics and catalysis took place in Mesilla, New Mexico, in February 2000. Six years later, what looked controversial then has become widely accepted. The basic enzymatic catalysis mechanisms, transition state binding[1] and ground-state destabilization,[2] are still accepted. What changed is a willingness to admit the possibility that motions of residues near the active site can have an effect on the catalytic mechanism and that should be taken into account in the interpretation of, for example, kinetic isotope effect (KIE) measurements.

These motions can influence the standard model of catalysis in different ways, presented in order of increasing controversy: (1) they may be extended motions related to conformational fluctuations; (2) they may be local subpicosecond motions near the active site; (3) they may force us to revise[3] our view of thermodynamic cycles often used to describe catalysis.[4]

In this review, we will discuss three kinds of dynamic effects.

1. "Rate-promoting" quasi-harmonic motions, a fast subpicosecond effect that we and others have proposed, usually for reactions that involve proton tunneling (sections 3.1 and 4.1).

2. Extended correlated motions involving several residues and the theoretical tools needed for studying them (sections 3.2 and 4.2).

3. Conformational fluctuations (section 5).

The structure of this review is as follows. In section 2, we will review the concept of "rate-promoting" vibrations. We will first need to review briefly the theory of quantum hydrogen/hydride transfer, because it is the large hydrogen mass (relative to an electron) that makes the reaction rate very sensitive to motions that modulate its transfer distance. We will then identify the experimental and computational signatures of these promoting vibrations.

In section 3, we will study lactate dehydrogenase (LDH). First we will identify promoting vibrations in this system. Then, we will identify other extended collective motions that affect catalysis, using transition path sampling, which allowed us to describe these collective motions in atomic detail.

In section 4, we will study purine nucleoside phosphorylase (PNP). First we will identify an unusual promoting vibration in this system, which acts through electron density fluctuations rather than transfer of a light particle. Then we will use essential dynamics to identify motions that increase turnover by facilitating substrate binding.

Finally, in section 5 we will briefly discuss recent work by other investigators (Truhlar, Gao, Brooks, and Hammes-Schiffer) on the relation of conformational fluctuations and

10.1021/cr0503052 CCC: $59.00
Published on Web 07/26/2006

Dimitri Antoniou received his B.Sc. in Physics from the University of Athens, Greece, in 1985, and his Ph.D. in Theoretical Condensed Matter Physics from Indiana University in 1991. He joined the Department of Biophysics in Albert Einstein College of Medicine in 1994 as a postdoctoral associate, and since 2001 he has been employed there as Research Faculty. His research interests include applications of methods of nonequilibrium statistical physics to chemical and biological systems.

Jodi Basner received her B.A. in Chemistry from the State University of New York at Binghamton. She received her Ph.D. in Computational Biophysics from the Albert Einstein College of Medicine in 2005. Currently, she is a postdoctoral research fellow at University of Maryland, working on nonequilibrium phenomena in biological systems.

Sara Núñez completed her B.Sc. in Organic Chemistry in the University of Barcelona and University College of London in 2000. She received her Ph.D. in Theoretical and Computational Chemistry from The University of Manchester in 2003. From 2003 to 2005, she was a postdoctoral associate at the departments of Biophysics and Biochemistry at Albert Einstein College of Medicine. She is currently working as a molecular modeler in the Discovery Team at Solvay Pharmaceuticals in The Netherlands.

Steven Schwartz received the B.A. degree from Columbia College of Columbia University in 1980. He received the Ph.D. from the University of California (Berkeley) in 1984. He was then a Member of Technical Staff at AT&T Bell Laboratories until 1993. He then joined the faculty of The Albert Einstein College of Medicine where he is now Professor of Biophysics and of Biochemistry and director of the Seaver Center for Bioinformatics. His research interests include quantum dynamics in condensed phases and the mechanism of enzyme reactions.

catalysis in dihydrofolate reductase, and we will close by proposing a new method for studying slow motions (such as conformational fluctuations) that may affect catalysis.

This review is not meant to be a comprehensive account of all work on enzyme dynamics and catalysis. The emphasis will be on the work done by our group, in two different aspects: (i) we will concentrate on fast subpicosecond enzyme motions, while other groups have studied mostly conformational fluctuations; (ii) we will present recently developed techniques (transition path sampling and essential dynamics) that can be used in studying the dynamics of enzymatic systems.

2. Proton Transfer and Rate-Promoting Vibrations

Previous research in which a rate-promoting vibration was identified in enzymatic systems involved a hydrogen transfer step via quantum tunneling (there are several excellent experimental reviews[5−8]). To understand why systems with hydrogen tunneling are good candidates for identifying promoting vibrations, we need to review the modern theory of quantum charge transfer in condensed phase, which we will summarize in this section.

2.1. Quantum Theory of Proton Transfer

Compared to gas-phase reactions, the reaction rate of proton transfer in condensed phases depends on the strength of coupling to the environment and, possibly, details of the dynamics of the environment. Because theories of quantum charge transfer in condensed phases were unavailable until the 1990s, out of necessity researchers were using simplified models. It is important to understand the limitations and validity range of the various theories that have been used. In the chronological order they appeared, they are: (i) the dynamics is over the barrier or just below the barrier, as described by transition state theory (TST; small quantum corrections); (ii) the dynamics takes place by tunneling from the ground state in the reactant well, as described by Marcus theory (large quantum effects); (iii) the dynamics takes place by tunneling from excited energy states in the reactant well (moderate quantum effects). Special care must be taken if one attempts to draw conclusions from the temperature dependence of the rate, because the rate has Arrhenius form

in all three regions, but the activation energy has different meaning in each regime.

2.1.1. Small Quantum Corrections (TST)

This region is often studied with the methods described in the book by Bell[9] (though the use of gas-phase corrections for a condensed-phase reaction is questionable). One assumes that between reactants and products there is a dynamical bottleneck (transition state), that there are several energy levels below the top of the barrier, and that the over the barrier transfer can be described by classical dynamics. The transition state theory result for the transfer rate is

$$k = \frac{k_B T}{2\pi} \frac{1}{Z_0} e^{-\beta V} \quad (1)$$

where $\beta = 1/(k_B T)$ is the inverse temperature and Z_0 is the partition function for an oscillator of frequency, ω_H. If we describe the motion at the reactant well quantum mechanically, then

$$\frac{1}{Z_0} = 2 \sinh\left(\frac{\beta\omega_H}{2}\right) \quad (2)$$

where ω_H is the reactant well frequency for a proton. If $\beta\omega_H/2 \ll 1$, one arrives at the familiar textbook TST result for the transfer rate, $k = (\omega_H/2\pi)\exp(-\beta V)$. However, a typical frequency for a proton−carbon bond vibration is 3000 cm^{-1}, so in the present case the opposite limit, $\beta\omega_H/2 \gg 1$, is relevant. In this limit, $1/Z_0 \simeq \exp(\beta\omega_H/2)$, and the semiclassical result for the rate is obtained,

$$k_H = A_H e^{-\beta(V-\omega_H/2)} \quad (3)$$

For C−H bond cleavage, eq 3 predicts a KIE equal to $k_H/k_D \approx 7$ at room temperature.

2.1.2. Large Quantum Effects (Marcus Theory)

When the energetic barrier is very high, tunneling takes place from the ground state. In this limit, the Marcus−Levich−Dogonadze theory[10] has been used in the study of electron transfer in solution and biomolecules. It is assumed that the environment can be described by an one-dimensional coordinate (a questionable assumption when details of environment dynamics are important), and one exploits the fact that in the deep tunneling limit the tunneling matrix element Δ can be used as a small parameter in a perturbative approach and finds a transfer rate equal to

$$k \approx \Delta^2 e^{-\beta(E_r+\epsilon)^2/(4E_r)} \quad (4)$$

where E_r is the reorganization energy of the environment, ϵ is the exothermicity, and Δ is the tunneling matrix element. In Marcus theory, the reaction coordinate is the environment coordinate, and the transition state is its value for which the proton potential energy surface (PES) is symmetrized.

Note that the quantum result eq 4 predicts an Arrhenius form for the rate, similarly to the TST result. In this theory, the KIE is equal to $k_H/k_D \approx \Delta_H^2/\Delta_D^2$, which in the deep tunneling limit has a value of the order 10^3-10^4, much larger than the measured KIE in biological systems. However, we will see later in this section that the Marcus theory approach, while valid for electron transfer, has to be modified for proton transfer.

2.1.3. Moderate Quantum Effects

This is the case when tunneling takes place from excited states, but not close to the barrier top, and it had eluded solution for decades. Finally, both numerical[11] and analytical[12] methods allowed solution in the 1990s.

It is instructive to investigate when and how the semiclassical theory fails. In Table 1, we compare some exact results[11]

Table 1. Comparison of Exact and Semiclassical Rates

$\omega_H/(k_B T)$	exact	semiclassical
3.2	0.8−1.8	1.5
4.8	2.0−3.8	2.3
9.6	30−1000	12.9

with the predictions of the semiclassical model eq 3. In Table 1, there is a range of values for the exact result, because the rate depends on friction (an effect that cannot be captured in the semiclassical model). We note that when the reactant frequency becomes large, the semiclassical theory of the rate fails (we should note that despite the failure in predicting the rate, the semiclassical model gives reasonably good prediction for the KIE).

We will now briefly describe our approach, known in the literature as the quantum Kramers problem. One assumes that the classical charge transfer problem is adequately described by the Langevin equation[13]

$$m\ddot{s} = -\frac{dV(s)}{ds} - \int_0^t dt' \, \gamma(t-t')\dot{s} + F_{env}(t) \quad (5)$$

where s is the reaction coordinate and $V(s)$ is the potential energy surface (PES). The influence of the enzymatic environment in eq 5 is represented by the random force, $F_{env}(t)$, which is related to the friction, $\gamma(t)$, through the fluctuation−dissipation theorem.[14]

A landmark result in rate theory was the proof[15] that the classical dynamics of s governed by the Hamiltonian (s is coupled bilinearly to a set of harmonic oscillators labeled by k)

$$H = \frac{p_s^2}{2m_s} + V(s) + \sum_k \frac{P_k^2}{2m_k} + \sum_k \frac{1}{2} m_k \omega_k^2 \left(q_k - \frac{c_k s}{m_k \omega_k^2}\right)^2 \quad (6)$$

is described by eq 5, when we integrate out the environmental degrees of freedom. The harmonic oscillators ω_k constitute a fictitious effective environment that is constructed to generate the correct friction kernel, $\gamma(t)$.

We must emphasize that there is no approximation in using harmonic oscillators to describe an anharmonic environment; these oscillators are an effective medium formed by the Fourier decomposition of the friction $\gamma(t)$ and are only indirectly related to protein dynamics. The advantage of casting the problem in terms of the Hamiltonian eq 6 is that there are many solution methodologies for this type of quantum Hamiltonian.

The Marcus−Levich−Dogonadze result eq 4 is the solution of the Hamiltonian eq 6 in the deep tunneling limit. In addition, the solution of the Hamiltonian eq 6 in the classical limit reproduces the transition state theory result, corrected

for recrossings of the barrier and for memory effects.[13] These results mean that the Zwanzig Hamiltonian provides a unified description of proton-transfer reactions in all three parameter regions defined earlier in this section.

Finally, we should mention that the approach described above is not the only possible one for studying quantum proton transfer in condensed phases. Truhlar and co-workers have followed a different methodology, based on variational TST, summarized in detail recently.[16]

2.2. Rate-Promoting Vibrations

The theory outlined in the previous subsection is appropriate for electron transfer but has to be modified for proton transfer. In this subsection, we will describe the physical justification and mathematical formalism that incorporates these effects.

2.2.1. Hynes's and Benderskii's Theories of Promoting Vibrations

Hynes and co-workers[17,18] noticed the following limitation of Marcus's rate theory eq 4 in their studies of proton transfer in solution in the early 1990s. If Q is the tunneling distance, it can be shown that the tunneling matrix element that appears in eq 4 has the form $\Delta \approx e^{-\alpha Q}$. For typical electron-transfer reactions, $\alpha \simeq 1$ Å^{-1}, while for typical proton-transfer reactions, $\alpha \simeq 30$ Å^{-1}.[17] This means that while electron-transfer rates are insensitive to variations of the tunneling distance Q, proton-transfer rates, because of the large value of α, depend strongly on motions that possibly reduce the transfer distance Q.

Hynes assumed that the deviation δQ of the transfer distance from its equilibrium value has a harmonic time dependence, $\delta Q = \delta Q_0 \cos(\Omega_{pv} t)$, and calculated the rate using Fermi's golden rule (i.e., the same level of approximation as Marcus's theory). He found for the rate

$$k = {\Delta_0}^2 \, e^{-\beta E_M} \, e^{2\alpha^2/(\beta M_{pv} \Omega_{pv}{}^2)} \qquad (7)$$

where Δ_0 is the tunneling splitting that corresponds to the equilibrium transfer distance, E_M is the activation energy of the ordinary Marcus theory, and M_{pv} and Ω_{pv} are, respectively, the mass and frequency of the promoting vibration.

In the previous subsection, we mentioned that Marcus's theory is not a plausible model for describing proton transfer because it predicts a KIE $k_H/k_D = \Delta_H{}^2/\Delta_D{}^2$, which is very large. This problem is remedied by Hynes's work, since the last term in eq 7 reduces significantly the KIE.

Hynes's formulation is intuitively very appealing, but there are some drawbacks. The environment is described by a one-dimensional coordinate, and the promoting vibration is introduced to modulate the tunneling splitting. In a series of papers on gas-phase proton transfer,[19−21] Benderskii had examined the same effect, that is, tunneling rate modulated by fluctuations of transfer distance, using a Hamiltonian formalism. We will briefly summarize his approach.

Let's assume a symmetric double well potential energy surface, $V(s) = as^4 - bs^2$. Its barrier height is $b^2/(4a)$, and the transfer distance is $\sqrt{2b/a}$. Let's assume that a harmonic mode $Q(t)$ is coupled to s through a term cs^2Q. Effectively, the parameter b of the original PES is replaced by $b - cQ(t)$. As $Q(t)$ oscillates, the transfer distance also oscillates around its equilibrium value. In addition, when the transfer distance decreases, the barrier height is lowered. In summary, the simple, symmetric with respect to s, functional form cs^2Q of the coupling reproduces the desired behavior of a PES whose barrier is lowered as the transfer distance decreases.

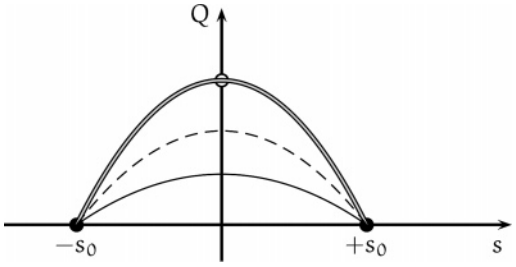

Figure 1. The potential energy surface in Benderskii's model. The dark circles are the reactant/product minima, and the open circle is the saddle point. The double line is the minimum energy path. The solid line is the instanton tunneling path for H, and the dashed line is that for D. Because D is heavier, it tunnels closer to the saddle point where the barrier is lower. As a result, the KIE is relatively low, even though the reaction proceeds through tunneling.

Benderskii solved this problem in the deep tunneling limit. We summarize Benderskii's results in Figure 1.

The double line represents the minimum energy path (MEP), which is the reaction path assumed by transition state theory. The single line represents the instanton trajectory (roughly, the most probable among the possible classical trajectories) for proton tunneling and the dashed line the instanton trajectory for deuteron tunneling. The heavier deuteron tunnels closer to the MEP, where the barrier is lower. These distinct instanton paths are the reason for the lowering of the KIE by the promoting vibration that we mentioned earlier.

There are other important features in this deceptively simple diagram. The instanton trajectories cross the TS parallel to the s-axis, which means that tunneling is happening instantaneously in the time scale of the promoting vibration. But this does not mean that the frequency of the promoting vibration does not play a role! In fact, the result depends on the ratio of the promoting vibration frequency over the barrier frequency, Ω_{pv}/ω_b. We have to distinguish between the following limits:[22]

- When $2\Omega_{pv}/\omega_b \ll 1$, we are in the "fast-flip" or "sudden approximation", or "corner-cutting" or "large curvature" limit, where the reaction coordinate follows the minimum energy path, but before it reaches the saddle point it tunnels along the s coordinate in a time that is short compared to the time scale of the Q vibration.
- When $2\Omega_{pv}/\omega_b \gg 1$, we are in the "slow-flip" or "adiabatic" or "small curvature" limit, where the Q vibration adiabatically follows the s coordinate and transfer takes place along the minimum energy path (i.e., at the saddle point).

Therefore, very fast promoting vibrations do not affect the rate, while we should expect to see their effect when $2\Omega_{pv}/\omega_b \ll 1$, that is, (for typical barriers) when Ω_{pv} is smaller than roughly 500 cm^{-1}, which explains why we mentioned earlier that we studied subpicosecond motions. This complicated behavior arising from the interplay of the coupled dynamics of the reaction coordinate and the subpicosecond promoting vibration cannot be captured by the simple versions of TST.

2.2.2. Theory of Promoting Vibrations in Condensed Phase

The formulation of promoting vibrations by Benderskii is very satisfactory because it cast the problem in a Hamiltonian

language. On the other hand, the Hynes formulation, even though it uses an ensatz for the promoting vibration, has the advantage that includes interaction with the environment (with the limitation of the Marcus model, that is, that the environment is represented by a single degree of freedom). We can incorporate these two theories into the Zwanzig Hamiltonian by adding a term, $cs^2Q + {}^1/_2M_Q\Omega_{pv}{}^2$, in eq 6, to obtain the Hamiltonian

$$\frac{p_s{}^2}{2m_s} + V(s) + cs^2Q + \frac{1}{2}M_Q\Omega_{pv}{}^2 + \sum_k \frac{P_k{}^2}{2m_k} + \sum_k \frac{1}{2}m_k\omega_k{}^2\left(q_k - \frac{c_k s}{m_k\omega_k{}^2}\right)^2 \quad (8)$$

This incorporates the advantages of Benderskii's and Hynes's ideas, and in addition contains a more realistic description of the environment. One important difference is that Hynes and Benderskii studied systems in which the oscillator Q was a bond vibration, while in eq 8, $Q(t)$ can be any variable that modulates the potential energy surface, for example, it can be a distance between the donor and a nearby residue that changes in time because of equilibrium fluctuations of the enzyme.

To establish a relationship between the Hamiltonian eq 8 and the actual enzymatic system, one performs a molecular dynamics simulation to obtain the force $F(t)$ acted upon the reaction coordinate. Then the force autocorrelation function $\langle F(t)F(0)\rangle$, which is proportional to the friction kernel $\gamma(t)$, is related to the parameters of the fictitious medium of eq 8 through

$$\gamma(t) = \frac{1}{k_BT}\langle F(t)F(0)\rangle \approx \sum_{k=1}^{N}\frac{c_k{}^2}{m_k\omega_k{}^2}\cos(\omega_k t) \quad (9)$$

This equation permits the mapping of the computed force $F(t)$ to the parameters of our Hamiltonian.

To obtain some insight into the behavior of the solutions of the Hamiltonian eq 8, we performed a numerical simulation of a model system:[23] we coupled s to 1000 harmonic oscillators ω_k with frequencies ranging from 10 to 1000 cm^{-1} and symmetrically to one oscillator Ω_{pv} with frequency 300 cm^{-1}. The PES was a symmetric double well potential that had barrier height equal to 6 kcal/mol and transfer distance 1 Å.

In Figure 2, we show the progress of the reaction coordinate from reactants to products. The very fast oscillations are bond oscillations in the reactant/product wells. The slower oscillation that envelopes the bond oscillations is the promoting vibration. Note that because the promoting vibration is fast, the time interval for which the barrier is lowered is not long enough for a reactive event to occur for each oscillation, that is, it requires several oscillations of the promoting vibration for the charge transfer to occur.

In Figure 3, we plot a statistics of the values of the promoting vibration coordinate as the reactive trajectories cross the transition state. The saddle point in Figure 2 corresponds to the value of Q shown with a dashed line in Figure 3. We note that the reactive trajectories do not pass through the saddle point, but rather through a broad region centered at the saddle point. This figure shows that the dynamics cannot be described by a single transition state.

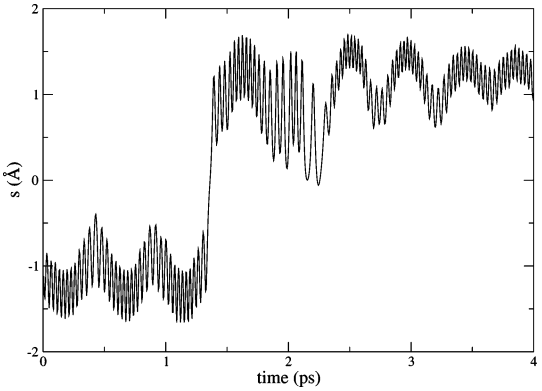

Figure 2. An example of a reactive trajectory. The transition state is at the $s = 0$ line, and the reactant/product wells are at the $s = \pm 1$ lines. For a subpicosecond rate-promoting vibration, several oscillations are needed to help the reactive event.

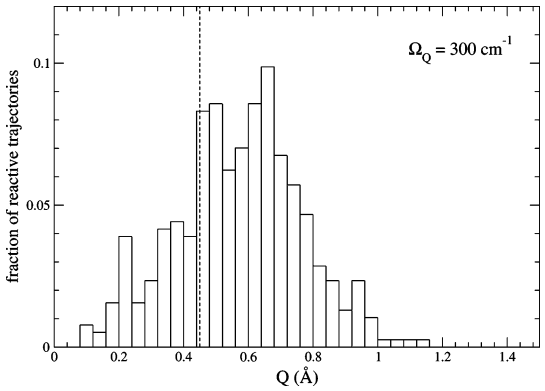

Figure 3. A histogram of the values of the promoting vibration coordinate Q, as the reactive trajectories cross the transition state. The dashed line corresponds to the location of the saddle point.

The deeper reason for this is that the assumption of separability fails:[24] the promoting vibration is strongly coupled to the reaction coordinate in the transition state region and the frequency of the promoting vibration is comparable to the inverted barrier frequency, so there is no separation of time scales.

Finally, in our opinion, there is an open question in quantum theories of proton transfer. The theories we have been discussing use a mean field potential as the potential energy surface. This is undoubtedly correct when the environment relaxes quickly in the time scale of the reaction. It has been argued[25,26] that the transfer step in quantum tunneling is very fast, and it is not certain that all the configurations that enter the mean field potential are sampled. In our calculations of model systems, we have seen that a typical time needed for the proton wave packet to tunnel is of the order of 1 ps. Even though this time scale is not as fast as suggested in the references above, certainly their argument has merit since there are protein motions that are slower than the time scale of proton tunneling.

2.3. Discussion

Since proteins are very anharmonic systems, one may ask what is the justification for modeling the protein environment as a set of harmonic oscillators in eq 8. The only approximation we have made is in modeling the proton transfer by the Langevin equation eq 5. One expects this to be a good approximation for the short time scales relevant for barrier crossing. Within the Langevin equation, the effect of the

environment on the proton is captured through the friction, which is obtained from a simulation and can be decomposed into Fourier components, which are the harmonic oscillators appearing in eq 8. That is, these oscillators are fictitious quantities introduced to reproduce the exact form of the friction, and no simplification regarding the protein anharmonic dynamics is made.

It is known from both experiments and computer simulations that if we embed a harmonic oscillator in a medium, it will be very quickly dephased, so one may wonder about the plausibility of identifying in an enzyme a promoting vibration with a well-defined frequency. In fact, the promoting vibration is not a harmonic oscillator embedded in the enzymatic environment. While the protein executes thermal fluctuations, we can record, for example, the distance $Q(t)$ between two residues. If the Fourier transform of $Q(t)$ is relatively peaked, then the distance between these residues varies in time like a damped harmonic motion. The promoting vibration $Q(t)$ is not a harmonic oscillator with specific energy levels, rather it is an internal distance (e.g., between residues that participate in the equilibrium fluctuations of the enzyme), which modulates the potential energy surface. In simple model calculations, we can mimic this effect by writing a Hamiltonian like eq 8 in which $Q(t)$ appears as an independent oscillator, but it must be understood that this Hamiltonian is a simplified model designed to produce a fluctuating PES, and $Q(t)$ is a quantity that parametrizes this fluctuation. One cannot assume beforehand that the distance $Q(t)$ is harmonic, one has to calculate its Fourier transform and check whether it is peaked at some frequency, as we will do in the examples in the next section.

Parenthetically, we should mention that highly anharmonic potentials do not necessarily exclude harmonic dynamics! An example is water: the interatomic potential is extremely anharmonic (hard spheres), but water supports harmonic waves (sound). The resolution of the paradox is that the variable that describes sound waves (density) is not the variable that enters the anharmonic interatomic potentials, so it is possible for equilibrium fluctuations, like sound, to have harmonic dynamics.

Finally, we should emphasize that promoting vibrations not only are coupled to the reaction coordinate, but also have similar time scale, picosecond, to the barrier crossing step. Therefore the effect of the promoting vibration is "dynamic", that is, to calculate the reaction rate one needs a detailed description of the full dynamics of the coupled reaction coordinate−promoting vibration system. Conformational fluctuations (whose time scale is much slower than tunneling) that enhance tunneling (to be discussed in section 5) are a "statistical" effect: the reaction rate is the sum of TST rates for barriers corresponding to some conformation weighted by the probability that the system reaches that conformation. This distinction between dynamic and statistical phenomena in proteins was first made in the classic paper of Agmon and Hopfield.[27]

2.4. Computational Diagnostic of Promoting Vibrations

In a realistic system, there are many other motions present, so there is no guarantee that the effect of the promoting vibration will not be masked by other interactions that are present in an enzyme. We need a diagnostic that will allow us to identify whether a promoting vibration is present when we perform a computer simulation of the dynamics of an enzyme.

We have found[28] such a computational signature in the framework of the Langevin equation, eq 5. Let's recall that if we compute from a simulation the force $F(t)$ on the reaction coordinate, then the friction kernel $\gamma(t)$ is proportional to the autocorrelation of that force. We have shown that if we add a term $cs^2Q + {}^1/_2M_Q\Omega_{pv}{}^2$ to the Langevin equation and allow the promoting vibration to be coupled to the environment with coupling strength ζ, the friction kernel becomes

$$\gamma_{pv}(t) = \gamma(t) + \frac{4c^2}{M\Omega_{pv}{}^2}s(t)s(0)\left[\cos(\tilde{\Omega}_{pv}t) + \frac{\zeta}{2\tilde{\Omega}_{pv}}\sin(\tilde{\Omega}_{pv}t)\right]e^{-\zeta t/2} \quad (10)$$

Here $\gamma(t)$ is the friction of the original Langevin equation and $\tilde{\Omega}_{pv} = \sqrt{\Omega_{pv}{}^2 - \zeta^2/4}$ is the effective frequency of the promoting vibration, modified due to its coupling to the environment.

Eq 10 provides the diagnostic we have been looking for. Note that the correction to the friction kernel due to the promoting vibration is proportional to $s(t)s(0)$. Suppose we perform a simulation where we have imposed constraints to keep the transferred proton fixed, while the correction term is proportional to $s(0)^2$. If we keep the proton fixed near the transition state $s = 0$, the correction term will be very small. If we keep it fixed away from the transition state (most simply, at the reactant or product configuration), the correction term will be nonzero. In addition, if we take the Fourier transform of eq 10, the presence of the trigonometric terms in the correction term will produce large peaks at the frequency of the promoting vibration.

In conclusion, the following is a computational diagnostic for the existence of promoting vibrations. One performs simulations with the transferred proton constrained first near and then away from the transition state; then one takes a Fourier transform of the calculated friction kernel; if one sees sharp peaks for the latter simulation that are absent when the proton was held fixed near the transition state, then this is evidence that a promoting vibration is present, and the position of the peak is an indication of its frequency.

2.5. Experimental Ramifications of Promoting Vibrations

The discussion in this section has suggested a possible experimental signature for the presence of promoting vibrations. Hynes's formalism, Benderskii's formalism, and our quantum calculations using the Hamiltonian eq 8 all predict a low KIE, that is, much lower than what one would expect for transfer by tunneling through a static barrier. In fact, the initial resistance to accepting that tunneling can occur in enzymes was exactly the low values of KIE. Hynes has recently reviewed[29] the influence of promoting vibrations on KIE with a perspective different than ours.

Furthermore, the tunneling rate depends exponentially on the reorganization energy of the environment, which for an enzymatic system depends strongly on the rigidity of the enzyme. This raises some intriguing possibilities for the interpretation of certain experiments on thermophilic enzymes. Thermophilic enzymes show low enzymatic activity at mesophilic temperatures, while the conservation of the active site structure and chemical mechanisms suggests that the same chemical mechanism is present at both thermophilic

and mesophilic temperatures. One possible interpretation focuses on the temperature-dependent motions of proteins, because experiments have shown that the rigidity of thermophilic proteins is more flexible at thermophilic than at mesophilic temperatures.[30]

The work that is of interest with respect to promoting vibrations is a study[31] of hydrogen tunneling in alcohol dehydrogenase from *Bacillus stearothermophilus*. The unusual features of this system are (i) the activation energy is smaller in the thermophilic regime, which in a naive interpretation would imply that tunneling is enhanced with increasing temperature, (ii) the primary KIE is small and temperature-independent in the thermophilic regime but larger and temperature-dependent in the mesophilic regime, and (iii) there is correlation between the rigidity of the protein (or specific subunits) and the temperature dependence of the transfer rates.[32,33] We have shown[34] that by assuming the presence of a promoting vibration in the thermophilic regime and assuming that it freezes out in the mesophilic regime, one is able to reproduce all the trends mentioned earlier in this paragraph. Reproducing trends is not definite proof, but at the very least it is a reminder that the presence of a minimal dynamical element makes the problem sufficiently complex that conclusions derived by studying Arrhenius plots can be misleading.

3. Lactate Dehydrogenase (LDH)

In this and the next section, we will present examples of enzymatic systems where we applied the ideas and formalism of the previous section and we were able to identify rate-promoting vibrations. The first system in which we identified a promoting vibration was horse liver alcohol dehydrogenase (HLADH). Because the results and analysis are similar to our analysis of LDH we present below, we refer the reader who is interested in the HLADH system to our original paper.[35]

Lactate dehydrogenase (LDH) catalyzes the interconversion of lactate and pyruvate with the coenzyme nicotinamide adenine dinucleotide (see Figure 4). This enzyme plays a fundamental role in respiration, and multiple isozymes have evolved to enable efficient production of substrate in different

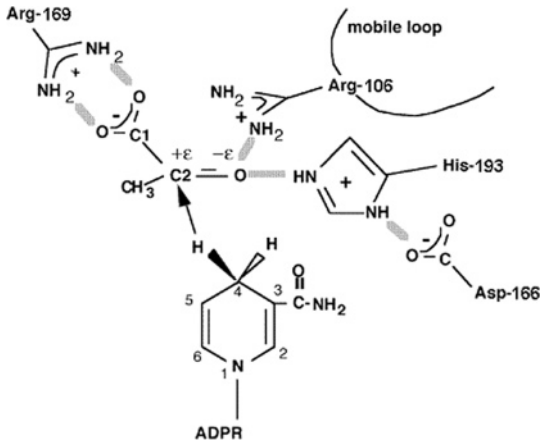

Figure 4. Diagram of the binding site of LDH with bound NADH and pyruvate showing hydrogen bonds between the substrate and key catalytically important residues of the protein. The catalytic event involves the hydride transfer of the C4 hydrogen of NADH from the pro-R side of the reduced nicotinamide ring to the C2 carbon of pyruvate and proton transfer from the imidozole group of His-193 to pyruvate's keto oxygen.

microenvironments. Two main subunits, referred to as heart and muscle, are combined in the functional enzyme as a tetramer, and subunit combinations range from pure heart to pure muscle. The kinetic properties of the heart and muscle isoforms are distinct: the heart favors production of pyruvate and the muscle of lactate. Despite this difference, the domain structure, subunit association, and amino acid content of the active sites of the two isoforms are almost identical, leading to the puzzle of what is the cause of their difference in activity.

3.1. Promoting Vibrations in LDH

In the following figures, the reactant configuration for the heart isoform is the line "lactate" and the product configuration is the line "pyruvate". And vice versa, the reactant configuration for the muscle isoform is the line "pyruvate" and the product configuration is the line "lactate".

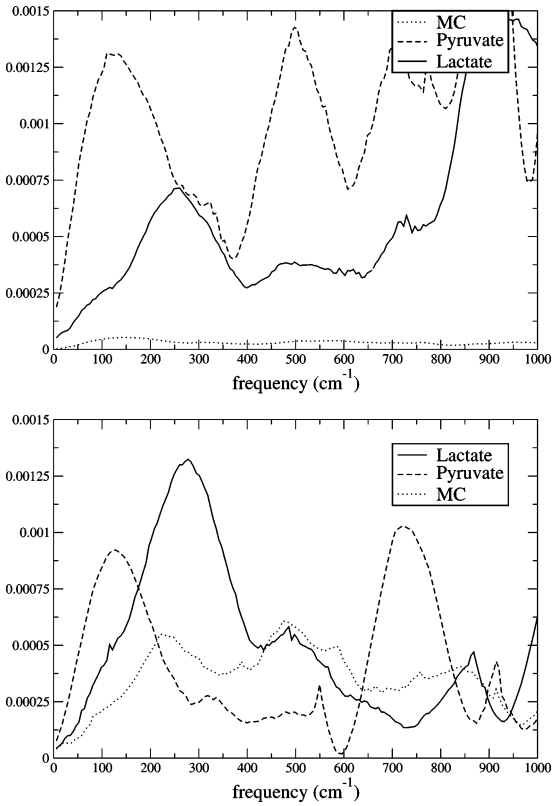

Figure 5. Wild-type heart LDH isoform: Fourier transform of the force on the reaction coordinate (top) and Fourier transform of relative donor−acceptance distance (bottom). As predicted by eq 10, the minimal coupling (MC) line has the lowest peaks. Whether the proton was held fixed at the reactant side (lactate line) or the product side (pyruvate line), there is an alignment of the low-frequency peaks of the spectra of the force on the reaction coordinate and the donor−acceptance vibration, suggesting a causal relationship between the two.

In Figure 5, we show results for the heart LDH isoform: the top panel is the Fourier transform of the force on the transferred hydride; the bottom panel is the Fourier transform of the relative motion between the substrate C2 carbon and carbon C4 of the nicotinamide ring of the cofactor NAD+/NADH. In Figure 6, we show the corresponding figures for the muscle LDH isoform. In these figures, we see clear evidence of the presence of a promoting vibration, according to the criteria outlined in the previous section:

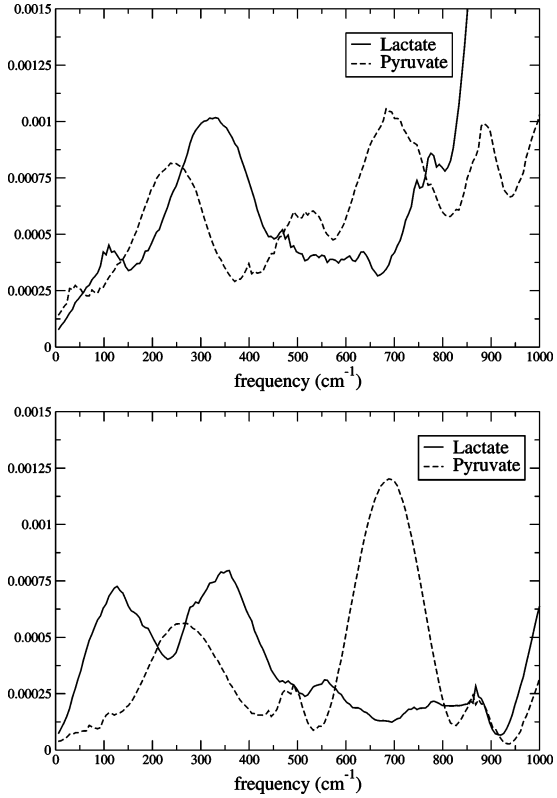

Figure 6. Wild-type muscle LDH isoform: Fourier transform of the force on the reaction coordinate (top) and Fourier transform of relative donor−acceptance distance (bottom). For the interpretation of the alignment of the low-frequency peaks, see Figure 5.

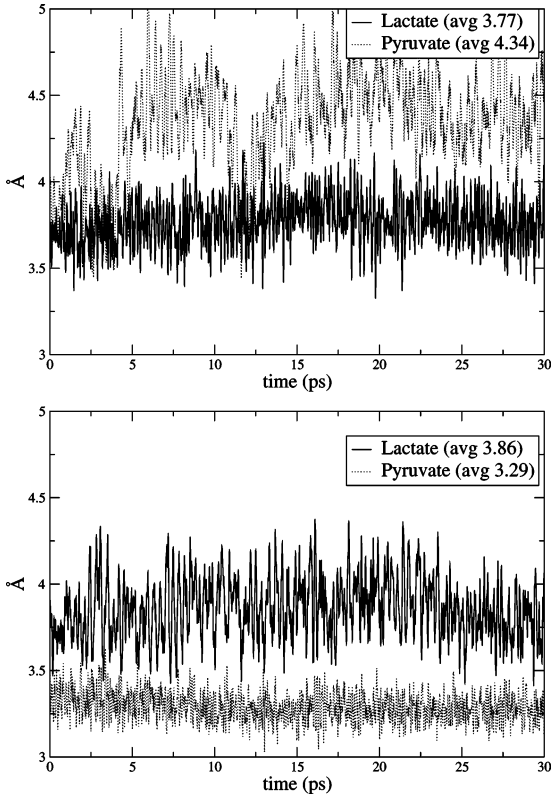

Figure 7. Donor−acceptor distance for the wild-type human heart lactate dehydrogenase isoform (top) and the muscle isoform (bottom).

1. The spectral density is much lower when the hydride is constrained near the TS, as predicted by eq 10 (minimal-coupling, MC, line in the figure).

2. The peaks of the Fourier transform of the force on the hydride are in resonance with the peaks of the Fourier transform of the relative donor−acceptor motion.

These results also contain information suggesting why one isoform favors production of pyruvate and the other of lactate. If we look at the peak around 200 cm^{-1}, the pyruvate peak is higher for the heart isoform and the lactate peak higher for the muscle isoform. Recall that the height of the spectral density is proportional to the force on the reaction coordinate. According to eq 10, a larger force could arise from a larger $s(t)$, that is, larger deviation from the TS. Since the lines "lactate"/"pyruvate" in Figures 5 and 6 correspond to the hydride bound to the donor/acceptor (and vice versa for the other isoform), it would be interesting to see what is the average distance of donor−acceptor in the two isoforms.

In Figure 7, we show the results of a 30 ps simulation for the donor−acceptor distance, that is, the distance between the C2 carbon of substrate and carbon C4 of the nicotinamide ring of the cofactor NAD+/NADH. Figure 7 shows that the average donor−acceptor distance is shorter for the heart isoform when lactate and NAD+ are bound and for the muscle isoform when pyruvate and NADH are bound. We propose that the different kinetic activity of the two isoforms is due to the reduced donor−acceptor distance when lactate is bound to the heart isoform and pyruvate is bound to the muscle isoform.

Finally, we mutated in silico residue 31, valine, to a less bulky one, alanine. If our interpretation is correct, we expect that the Fourier transform of the force on the hydride would have a higher peak in the wild type than in the mutant, since the bulkier valine is more efficient in pushing the nicotinamide ring of the NAD^+, and as a result the average donor−acceptor distance would be smaller for the wild type than for the mutant. In Figure 8, we show the results of the simulation, which are consistent with our prediction. As we mentioned earlier, the peak of the spectral density can be lowered either because the coupling to the reaction coordinate is weaker or because the reaction coordinate is fixed closer to the transition state. The bottom panel of Figure 8 shows that the average donor−acceptor distance is larger for the mutant result; therefore the lower peak of the spectral density in the top panel necessarily means that the coupling is weaker for the less bulky alanine.

3.2. Description of Correlated Protein Motions in Atomic Detail: Transition Path Sampling

We now turn our attention to other kinds of correlated protein motions (with picosecond or nanosecond time scales) and methods that can identify them. The rate-promoting vibrations we examined earlier are just one example of correlated protein motions. Because promoting vibrations involve residues in the immediate vicinity of donor and acceptor, it was relatively easy to identify them. In the more general case of extended correlated motions, it is a challenge to identify residues that take part in them. We will describe a method that we have successfully used for identifying atomic motions of interest, the transition path sampling.

3.2.1. Transition Path Sampling

Transition path sampling (TPS) was originally developed for studying rare reactive events. One of the most difficult problems in studying reactive events is to define an appropriate reaction coordinate and find the location of the

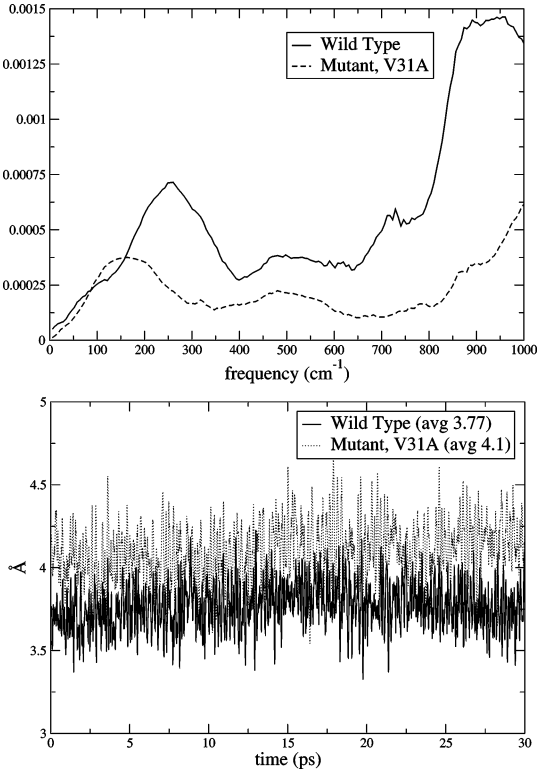

Figure 8. (top) Spectral density for the reaction coordinate in the wild type and mutant human heart lactate dehydrogenase isoform with lactate and NAD+ bound: the solid line is the wild-type configuration where residue 31 is valine, and the dashed line is the mutant configuration where residue 31 is alanine. (bottom) Donor−acceptor distance for the wild type and mutant human heart lactate dehydrogenase isoform with lactate and NAD+ bound: the solid line represents the wild-type configuration where residue 31 is valine, and the dashed line represents the mutant configuration where residue 31 is alanine.

transition state. In addition, if one tries to simulate rare reaction events using a molecular dynamics simulation, most of the trajectories that start from the reactants will not cross to the products, and as a consequence the calculation becomes computationally infeasible, because the time step that must be used in the MD simulation is much smaller than the time scale of interest.

Transition path sampling (TPS)[36,37] addresses these problems by performing a Monte Carlo search in the trajectory space. It can simulate rare events without the knowledge of a reaction coordinate or the transition state. Note that TPS is an algorithm for searching the trajectory space and requires a separate algorithm (molecular dynamics) to generate the trajectories themselves. The essence of TPS is that the chaotic nature of classical multidimensional systems guarantees a fast Monte Carlo search of the trajectory space.

A brief description of the algorithm follows (see Figure 9). Let us assume a transition between R and P (i.e., reactants and products). Since R and P are long-lived states, they can accommodate equilibrium fluctuations and can be characterized by a variable, called "order parameter", which can be used as a criterion for deciding whether the system is localized in R or P. Let us further assume that we somehow know one reactive trajectory that starts from R and ends in P. In the TPS algorithm, we randomly select a time slice along this reactive trajectory, we perturb slightly the momenta at that time slice, and starting from that time slice and using the new momenta, we propagate ("shoot") forward

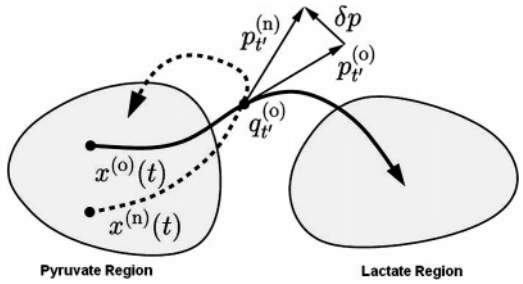

Figure 9. Schematic representation of the TPS algorithm. The shaded regions are identified by the order parameter as reactants and products. The solid line is a reactive trajectory. A "shooting" move is shown: a time slice q_t was chosen along the reactive trajectory, momenta p_t were perturbed, and then the system was propagated forward and backward in time, resulting in a nonreactive trajectory shown with the dashed line.

and backward in time, examining whether the new trajectory is reactive or not. In the usual Monte Carlo fashion, the new trajectory is accepted or not, according to some probability distribution. Because of the ergodicity of classical dynamics, new trajectories are expected to quickly deviate from old ones, leading to a fast sampling of the trajectory space.

3.2.2. An Ensemble of Reactive Trajectories in LDH

We have applied[38] the transition path sampling algorithm to LDH, that is, to the enzyme in which we identified a rate-promoting vibration, as discussed earlier. This work, along with a paper by Schlick,[39] were the first that applied the TPS algorithm to a realistic protein.

By finding common features in all the harvested trajectories, one can get insights for defining an appropriate reaction coordinate and for identifying experimental targets for future studies. Recall that LDH catalyzes the interconversion of the hydroxy-acid lactate and the keto-acid pyruvate with the coenzyme nicotinamide adenine dinucleotide. The reaction involves a double transfer: a proton transfer between the active site histidine and the C2 substrate oxygen and a hydride transfer between NC4 of the coenzyme and C2 of the substrate (see Figure 4). In fact, there was a controversy regarding whether the transfer steps are concerted or sequential that our study was able to resolve. Since the reaction involves bond cleavage, we must use a quantum potential for describing the reactive potential surface. The details of our choice for the quantum description are explained elsewhere.[38] Below we briefly define the variables and concepts that our TPS simulation used.

1. Definition of the Order Parameter. The first step in the TPS algorithm is to define an "order parameter", that is, a variable that describes whether the system is in the reactants, the products, or an intermediate region, as shown schematically in Figure 9. The pyruvate and lactate regions were defined by the values of the appropriate bond lengths.[38] The pyruvate region included all configurations where the bond length of the reactive proton and the reactive nitrogen of the active site histidine was shorter than 1.3 Å and the bond length of the reactive hydride and the reactive carbon of the NADH coenzyme was shorter than 1.3 Å. The lactate region included all configurations where the bond length of the reactive proton and the reactive substrate oxygen was shorter than 1.3 Å and the bond length of the reactive hydride and reactive substrate carbon were shorter than 1.3 Å. The bond lengths were determined as the maximum over a 4 ps trajectory in each substrate region. A reactive trajectory was

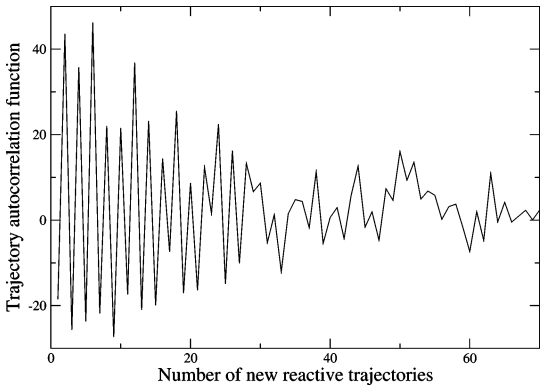

Figure 10. Autocorrelation function for trajectories plotted vs the number of reactive trajectories that have been generated after a given trajectory. The figure shows a decorrelation of reactive trajectories generated by TPS.

defined as a single dynamics simulation, which connected the pyruvate region to the lactate region or vice versa.

2. Decorrelation of Trajectories. The goal of TPS is to generate reactive trajectories that span the whole trajectory space. We must ensure that the ensemble of trajectories we generated do not lie "near each other" in the trajectory space. The variable that monitors this is an autocorrelation function of the appropriate variable. This autocorrelation function is shown in Figure 10. As can be seen, the trajectories became uncorrelated after about 30 successful iterations of the algorithm.

3.2.3. Results: Atomic Description of Relevant Catalytic Motions

1. Concerted versus Stepwise Transfers. We now address the question of whether the hydride and proton transfers are concerted or whether the hydride transfer precedes the proton in the pyruvate to lactate reaction direction. Our TPS study showed that both mechanisms are possible. In Figure 11, we show the distribution of the time

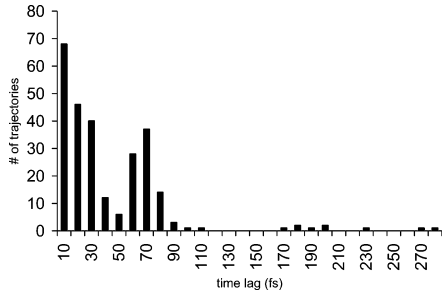

Figure 11. Distribution of the time lag between the hydride and proton transfer.

lag between the hydride and proton transfer for all reactive trajectories. We note that both concerted and sequential transfers are possible and that 74% of the trajectories have a time lag greater than 10 fs, indicating that the majority of reactive trajectories have sequential transfer steps.

2. A Compression of Residues Facilitates Catalysis. We have identified a compression−relaxation sequence of residue motions that facilitates catalysis. These are the residues 31 and 65, located behind the cofactor and transferring hydride, and residues 106 and 195, located on the acceptor side behind the substrate.

Figure 12 is helpful in identifying the location of important residues near the active site. In Figure 13, we plot various

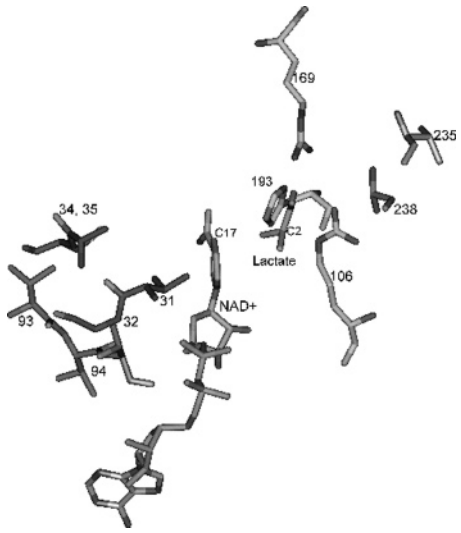

Figure 12. Location of various residues near the active site.

distances that reveal a compression of residues that occurs close to the reaction event. They are taken from a trajectory with a concerted hydride and proton transfer, but the results are the same for trajectories that had sequential transfers. All graphs are plotted in the pyruvate to lactate reaction direction.

When the donor−acceptor distances for the hydride and proton transfers reach their minimum (around time = 6130 fs in panels b−d, Figure 13), interactions across the donor, transferring atom, and acceptor are initiated. The events that occur next (after time = 6130 fs) are critical for the completion of the reaction. The continued compression of the donor side residues (panel c) toward the active site are involved not only with bringing the donor−acceptor distance closer together but also with shifting the entire enzyme. While the donor−acceptor distances increase again, it will be the motion of the surrounding residues that ultimately determine whether the atoms transfer. In particular (as shown in panels c and d, Figure 13), the compression of the donor side residues causes the acceptor side residues to relax away and the reaction to complete.

4. Human Purine Nucleoside Phosphorylase (hPNP)

4.1. Promoting Vibrations in PNP

Up to this point, all the examples we discussed concerned protein motions that affect reactions that involve a light particle transfer. However, rate-promoting enzymatic motions can also exist in other types of reactions. For example, we have shown[40] that such motions can influence catalysis by acting through electron density fluctuations caused by geometrical changes. The system we investigated is human purine nucleoside phosphorylase (hPNP), which catalyzes reversible bond cleavage of 6-oxopurine nucleosides to form phosphorylated α-D-ribose products in the presence of phosphate, as seen in Figure 14.

The cleavage of the C-1′−N-9 ribosidic bond (for atom terminology, see Figure 15) occurs in a dissociative mechanism that forms a TS with a substantial oxycarbenium ion character. The phosphate provides an electrostatic stabilization of this oxycarbenium ion, encouraging TS formation.[41,42] In summary, oxycarbenium stabilization, increased phosphate

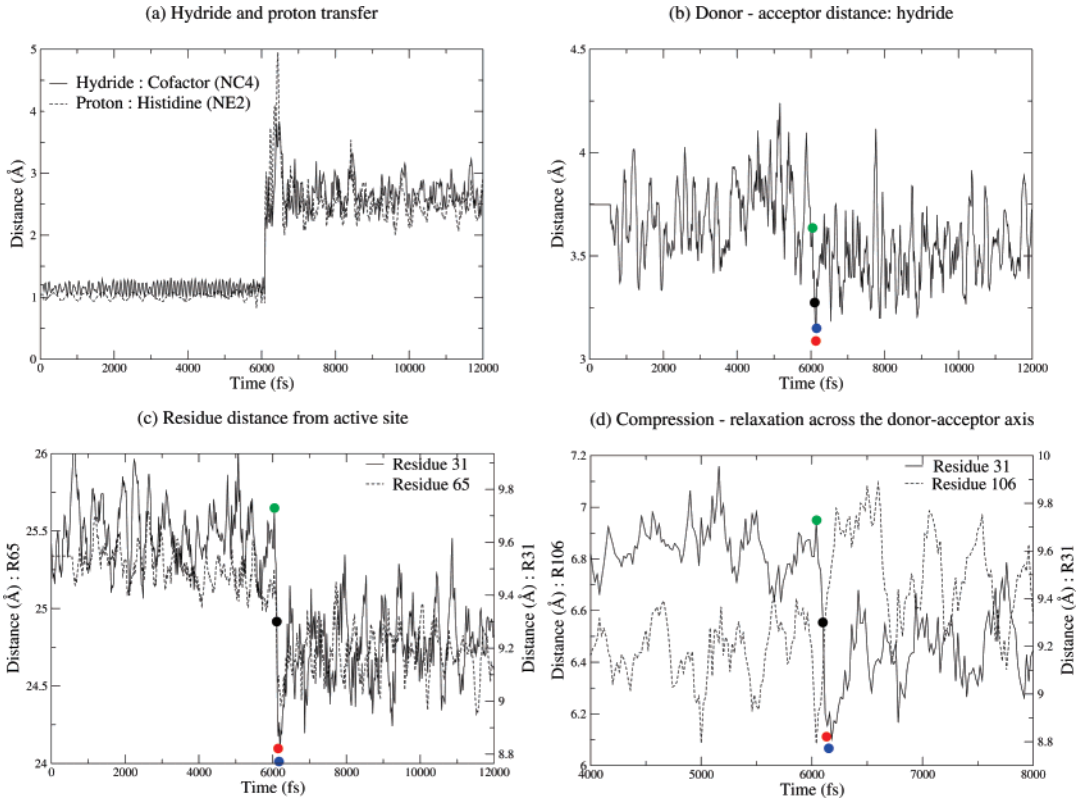

Figure 13. Comparison of motions of donor−acceptor and surrounding residues reveals a compression−relaxation motion. Panel a plots the distance of the hydride from the cofactor reactive carbon and the distance of the proton from the histidine reactive nitrogen. At time = 6100 fs, the atoms begin to transfer to the substrate. Panel b plots the donor−acceptor distance for the hydride. The four color solid circles around time = 6130 fs represent when certain distances reach their minimum. These minimum distances are (green) distance of arginine 106 from the active site, (black) proton donor−acceptor distance, (blue) hydride donor−acceptor distance, and (red) distance of valine 31 from the active site. A similar plot can be drawn for the proton transfer. Panel c plots the distance of residues 31 and 65 from the active site. They are located behind the cofactor and transferring hydride. The four color solid circles have the same meaning as those in panel b. Panel d plots the distance of residues 31 and 106 from 4 to 8 ps. Residue 106, responsible for polarization of the substrate carbonyl bond via hydrogen bonding, initially compresses toward the active site reaching a minimum distance at 6043 fs. By 6153 fs, residue 31 has reached its minimal compression toward the active site. The four solid circles have the same meaning as those in panel b. The donor side residues pass through their minimum in the pyruvate basin about the time the minimum proton donor−acceptor distance is reached (i.e., proton donor−acceptor minimum is mainly achieved through the acceptor side residue compression toward the active site). The continued compression of the donor side residues toward the active site, while the acceptor side residues resume an oscillation, brings the hydride donor−acceptor residues together and pushes the acceptor side residues away from the active site.

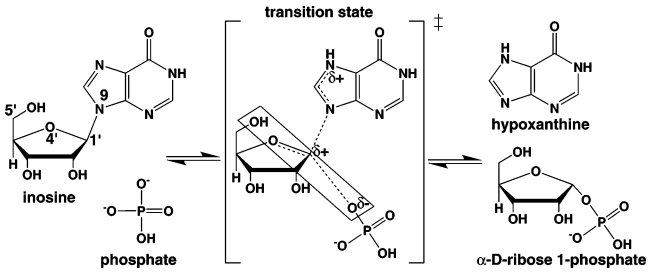

Figure 14. hPNP-catalyzed phosphorolysis of the purine nucleoside. The guanine leaving group and phosphate nucleophile are well-separated from the oxycarbenium ion, defining a highly dissociative TS. Note the oxygen stacking, indicated by the rectangle, of O5′, O4′, and the phosphate nucleophile, O_P.

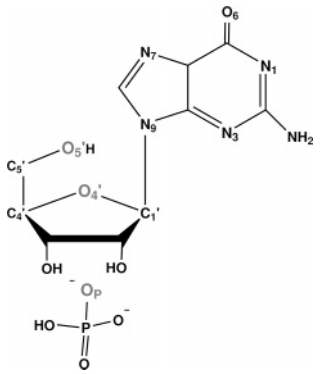

Figure 15. Atomic nomenclature of the purine nucleoside and phosphate nucleophile.

ionization, and purine ring activation contribute in concert to catalytic acceleration. Crystallographic data of several hPNP complexes with TS analogues showed an unusual geometric arrangement of the atoms O-5′, O-4′, and O_P, lying in a close three oxygen stack (Figure 15), which was later corroborated by extensive experimental kinetic isotope effect (KIE) analysis.[43] We will present evidence that protein motions in hPNP and its substrates cause the O-5′, O-4′ and O_P oxygens to squeeze together and push electrons toward the purine ring, stabilizing the oxycarbenium character of the TS. As the N-ribosidic bond is cleaved, electron density is expelled by the oxygen-stack compression toward the purine ring, and this improves electrostatic interactions with nearby residues and facilitates the abstraction of a proton from a close-by proton donor, making the purine a better leaving group and accelerating catalysis. Details of the computations can be found in the original publication.[40]

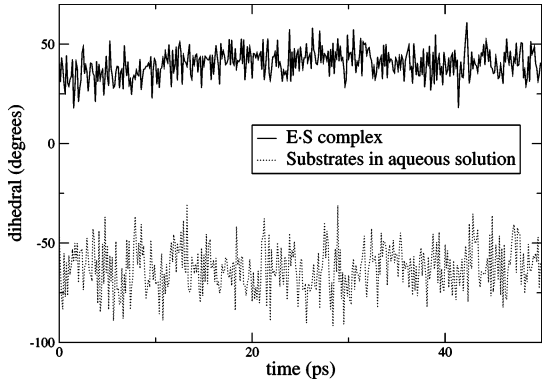

Figure 16. O-5′−C-5′−C-4′−O-4′ dihedral of the ribose ring during the WT classical MD simulation in aqueous solution and in the E·S complex.

4.1.1. Results: Dynamics

From a classical MD simulation, we calculated the time series for the O-5′−O-4′ and O-4′−O_P distances and found that these distances are quite stable, deviating only up to 0.3 Å from their average value. This implies that the O-5′−C-5′−C-4′−O-4′ dihedral is not rotating freely as it does in aqueous solution but is restricted by the enzymatic environment. We show the time series for that dihedral in both the enzymatic environment and aqueous solution in Figure 16. We note that the mean value in each case is different and that there is a higher deviation from the mean value in solution, verifying that this dihedral's motion is restricted in the enzyme.

Table 2. Average O-5′−O-4′ and O-4′−O_P Distances (Å) for the WT and Mutated hPNPs

distance	WT	E201G	V260G	H257G
O-5′−O-4′	2.81 ± 0.08	2.88 ± 0.11	2.78 ± 0.08	3.04 ± 0.08
O-4′−O_P	4.34 ± 0.10	6.58 ± 0.11	3.90 ± 0.11	4.69 ± 0.10

In Table 2, we show the average O-5′−O-4′ and O-4′−O_P distances and standard deviations for the WT and for several mutants of hPNP complexed with guanosine and phosphate (the maximum fluctuation of the O-5′−O-4′ distance is 0.6 Å; therefore a difference of, e.g., 0.2 Å in the average distance is substantial). For each mutation, the changes in compression of the oxygen stack were different. For example, we found that for the H257G mutant, the average O-5′−O-4′ distance was considerably higher than that of the WT, meaning that the residue H257 plays a role in keeping the two oxygens compressed. In Figure 17, we show the location of the residues E201, V260, and H257.

We now present a dynamical analysis of the time series for these distances. In the top panel of Figure 18, we show the Fourier transforms of the O-5′−O-4′ distance autocorrelation function and of the O-5′−O-4′, O-4′−O_P distance−distance correlation function. The spectra are very similar, indicating that O-5′−O-4′ and O-4′−O_P oscillate at the same frequencies in the enzyme environment, 125 and 465 cm^{-1}.

Next we examine whether these vibrations are unique in the enzymatic environment or they are inherent in the substrates. In the top panel of Figure 19, we compare the calculation in the enzyme (dashed line) with a simulation of the substrates in aqueous solution (solid line) in the absence of hPNP. The spectrum of the O-5′−O-4′ distance autocorrelation function of solvated substrates showed a peak at 330 cm^{-1} and of the unsolvated substrates at 285 cm^{-1}, that is,

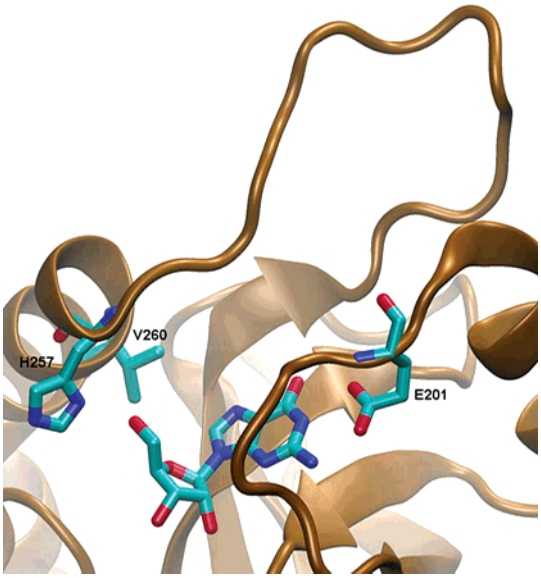

Figure 17. Location of residues E201, V260, and H257 relative to the substrate.

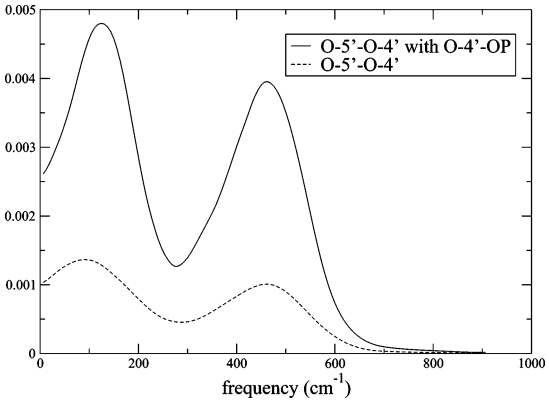

Figure 18. Comparison of the spectra of the O-5′−O-4′ distance autocorrelation function and the O-5′−O-4′ and O-4′−O_P distance−distance correlation function.

distinct from the peaks in the presence of the enzyme, proving that hPNP is directly affecting the way in which these oxygens naturally vibrate.

To assess the effect of the mutation of nearby residues on the three-oxygen stack electronic interaction, we performed classical simulations of mutated hPNPs. We studied whether changes in protein structure have an influence on the pattern of spectra discussed above for WT hPNP. In particular, we mutated F200G, E201G, H257G, H257A, V260G, and L261G. The spectrum of the O-5′−O-4′ motion for the F200G, E201G, V260G, and L261G mutated hPNPs was very similar to that of the WT, but as can be seen in the bottom panel of Figure 19, the spectrum for the H257G hPNPs was very similar to that of the unsolvated substrates. These results show that H257 is responsible for modifying the power spectrum in the E·S complex.

4.1.2. Results: Energetic Barrier

Using the hybrid QM/MM method described in the original publication,[40] we obtained the potential energy surfaces for the phosphorolysis reaction for various E·S complexes for a range of O-5′−O-4′ and O-4′−O_P interatomic distances. In the original publication, we presented detailed results for the activation energies as a function of

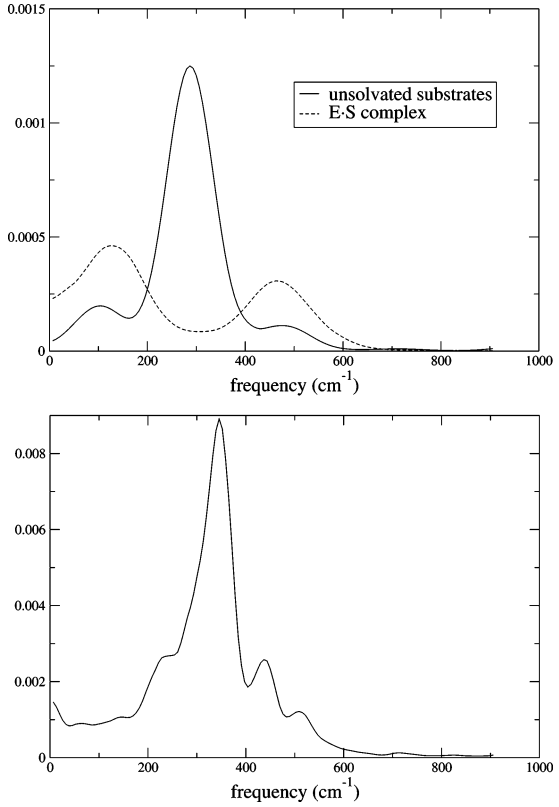

Figure 19. (top) Spectra of the O-5′−O-4′ distance autocorrelation function for hPNP and unsolvated substrates. Note that the natural vibration of the oxygen centers, that is, 285 cm^{-1}, is altered in the presence of the enzyme. (bottom) The power spectrum of the H257G mutant of the E·S complex shows a distinct peak at 333 cm^{-1}, very similar to the result for the solvated substrate.

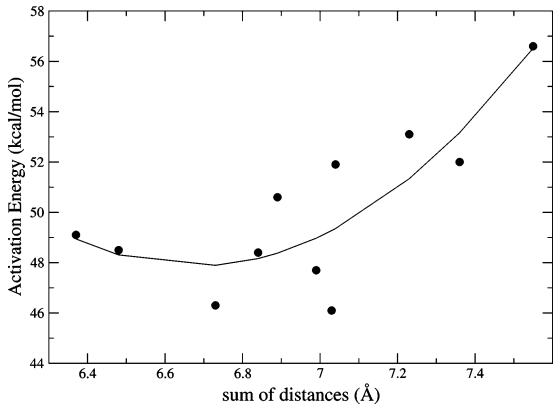

Figure 20. Activation energies (kcal mol^{-1}) versus the sum of O-5′−O-4′ and O-4′−O_P distances (Å) for the E·S complex.

oxygen interatomic distances of the E·S complex and the E·TS complex. This collection of structures covered a wide range of geometries with O-5′−O-4′ ranging from 2.78 to 3.64 Å and O-4′−O_P ranging from 3.35 to 4.30 Å. Thus, these structures were sufficient to represent the different E·S geometries that can be found in the PES.

We fitted the calculated activation energies to a function that had up to quadratic terms, as seen in Figure 20 (a parabolic fitting had smaller χ^2 than the also plausible linear fitting). The parabolic dependence of the activation energy on distance may have a simple interpretation: as the distances between the oxygens increase the energy rises as carbocation stabilization is lost, but at shorter distances, as we approach distances equal to twice the van der Waals radius, electron−electron repulsion will compete with the stabilization, and there is a point where there are no further reductions of the activation energy. From the values of the curvature of the parabolic fittings, we can obtain a spring constant, and by using a mass equal to the reduced mass of O−O, we can obtain an effective harmonic frequency associated with the parabolic fittings shown in Figure 20. This effective frequency was equal to 180 cm^{-1}, in surprising agreement with the position of the peaks of the spectra of the oxygen motions.

In conclusion, the protein motion that compresses the oxygen stack is one of the factors that makes the reaction possible, leading up to a 20% decrease in barrier height.

4.2. Motions that Facilitate Substrate Binding: Essential Dynamics

We found above that protein motions in hPNP accelerate the chemical step. In our study of this enzyme, we were able to identify motions that increase turnover by creating substrate binding affinity. In particular, we have studied[44] the conformational change in the 241−265 loop and identified variations in its orientation that are crucial in determining the substrate accessibility to the active site. In our studies, we used the essential dynamics method, which we briefly review below.

4.2.1. Essential Dynamics (ED)

Essential dynamics (or principal component analysis) is a method commonly used for identifying large scale motions in proteins, for example, protein folding or substrate binding. A summary of the method follows. Let $\vec{R} = (R_{1,x}, R_{1,y}, ..., R_{N,z})$ be the positions of the protein atoms. One assumes that the solution of Newton's equation of motion can be written in the following approximate form:

$$\vec{R}(t) \simeq \sum_{m=1}^{3N} a_m(t)\vec{\eta}_m \tag{11}$$

One then tries to find the coefficients and basis functions a_m and $\vec{\eta}_m$ that provide the best approximation (in a least-squares sense) of $\vec{R}(t)$ to the exact solution of Newton's equation of motion. This condition is satisfied by choosing the spatial basis set $\vec{\eta}_m$ to be the eigenfunctions of the covariance matrix

$$C_{ij} = \langle (R_i - \langle R_i \rangle)(R_j - \langle R_j \rangle) \rangle \tag{12}$$

where $\langle ... \rangle$ denotes time average over the entire MD trajectory. When a few eigenvalues of the covariance matrix are much bigger than the rest, the corresponding eigenvectors dominate the dynamics. When sorted by their eigenvalues, the ED modes are sorted according to their contribution to the total mean-square fluctuation. These few dominant modes are designed to provide a good fitting to the trajectory. In a protein, there may be concerted motions of groups of atoms (e.g., loop motions) that provide a significant number of covariant matrix elements, C_{ij}, and therefore dominate the principal eigenvectors of the covariant matrix. In this case, essential dynamics separates the conformational space into an essential subspace containing only a few dominant collective modes and a remaining space, which contains random atomic fluctuations.[45,46]

4.2.2. Substrate Binding in PNP

Experimental results led us to focus our attention on the 241−265 loop. If one assumes that each X-ray crystal

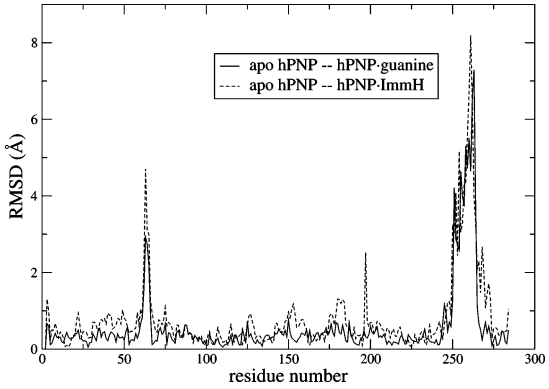

Figure 21. Detailed root-mean-square displacement (RMSD), per residue, of the geometric difference between the apo hPNP−hPNP·guanine (solid) and apo hPNP−hPNP·ImmH (dashed) crystal structure pairs. The different RMSDs of both pairs of crystals provide evidence that the TS analogue is bound to hPNP much more tightly than the substrate analogue.

structure represents a possible conformation in solution, considering several crystals and their relative atomic *B*-factors presents an experimental view of the conformational flexibility of the protein at an atomic resolution. The relative *B*-factors of the C_α atoms of apo hPNP and hPNP complexed with the transition state analogue immucillin-H show that the loop residue E250 is the centroid of highly mobile region, while residues G63 and E183 are centroids of more localized mobile regions. Additionally, from the structural differences between the crystal pairs of apo hPNP−hPNP·guanine (formation of the Michaelis complex) and apo hPNP−hPNP·ImmH (formation of the TS analogue complex), it has been questioned whether correlated motions exist to allow the necessary conformational change of the 241−265 loop for substrate binding and turnover. It is accepted that reorganization of this flexible loop, which makes up part of the active site, is essential for allowing different substrates/inhibitors to enter the active site.[47] The loop displacement is conjectured to push the substrates toward the active center favoring more reactive configurations. In Figure 21, we show the root-mean-square deviation of the C_α geometric difference between the apo hPNP−hPNP·guanine and the apo hPNP−hPNP·ImmH pairs. The same geometrical difference trend appears for any combination of two apo hPNP structures with six substrate/TS analogues, confirming the substantial loop rearrangement upon substrate analog/transition state analogue binding.

We used principal component analysis to identify correlated motions in different forms of hPNP, namely, its apo and complexed forms, and assess whether they facilitate the 241−265 loop rearrangement prior to the subsequent phosphorolysis reaction and compared the results to the crystallographic *B*-factors. Finally, via experimental site-directed mutagenesis, several residues implicated in the correlated motion were mutated, and the kinetic constants k_{cat} and K_M (fingerprints of catalytic efficiency) were measured[44] to weigh the impact of these residues in the phosphorolytic efficiency.

4.2.3. Results: Mobile Residues in the Active Site

We performed molecular dynamics simulations for the APO, ES, and EI−APO models. The objective of the EI−APO simulation is to capture putative concerted motions in hPNP during the loop conformational change taking place upon going from an "E·I geometry" toward an "apo hPNP geometry", which reversibly translates into existing motions in hPNP during substrate binding and TS formation.

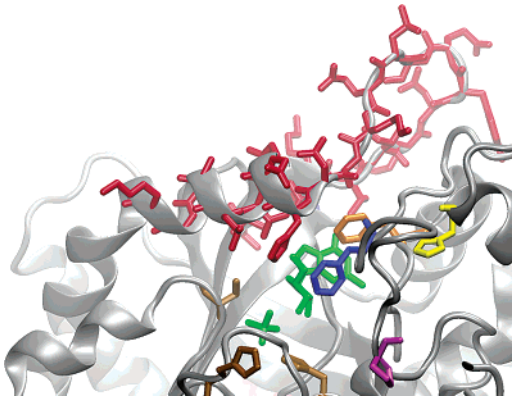

Figure 22. hPNP with marked residues that show correlated motions: S33 (brown), H64 (brown), H86 (brown), P150 (magenta), F159 (blue), H230 (yellow), F200 (orange), and 241−265 loop (red).

The three computational models (APO, ES, and EI−APO) present distinct characteristics in their correlated motions. Some similarities are found, for example, in the high mobilities of G63 and E183, in agreement with their high crystallographic *B*-factors. However, other residues that had not been seen as highly mobile based on their *B*-factors (namely, F159, P150, H230, and F200) have been found to have correlated dynamics. This implies that observation of crystallographic structures alone may not be enough to infer important dynamic behavior in proteins and that additional MD studies are needed to identify correlated dynamical modes.

We found correlated motions on the 241−265 loop, particularly present in the simulations of the Michaelis complex, and in a lesser extent in the EI−APO simulations. This suggests that the loop may have a favorable role in capturing the substrate as well as in the chemical step. Figure 22 highlights the residues that were identified by the principal component analysis: note the presence of residues F159 and F200, whose involvement in binding was not obvious from *B*-factors alone.

4.2.4. Experimental Site-Directed Mutagenesis

The X-ray crystal structures indicate that all direct contacts between hPNP and the substrates guanosine and phosphate are through amino acid side chains. Our site-directed mutagenesis strategy replaced each residue with glycine to assess the contribution of the residue's side chain to substrate binding, catalysis, or both. Results from the kinetic studies (Table 3) indicate that substrate binding affinity was most

Table 3. Experimental Kinetic Parameters for Different Mutants, Which Show Correlated Motions in hPNP

		mutant			
	WT	F200G	F159G	H230G	N121G
K_M (μM)	76.8	1580	2260	145	64.9
k_{cat} (s^{-1})	32.4	3.8	2.3	2.6	33.0
k_{cat}/K_M	4.2	0.024	0.01	0.1	5.0

sensitive to the F159G and F200G mutations. In the phosphorolytic direction, an increase of ca. 400-fold in K_M (and modest change in k_{cat}) is observed for the F159G mutant. Loss of the herringbone-type interaction between the β-face of the ribose and the hydrophobic surface created by this

residue is important for substrate binding, thus essential for hPNP activity. Additionally, the H230G mutant showed modest changes in both K_M and k_{cat}, despite its long distance from the active site. Finally, the N121G mutant did not show any relevant change in catalytic efficiency, even though it had substantial concerted dynamic behavior during the Michaelis complex simulation.

5. Conformational Fluctuations

The motions we examined in the previous sections had picosecond or nanosecond time scales; therefore they were accessible with ordinary molecular dynamic simulations. However, it is well-known that conformational fluctuations are sometimes coupled to the reaction coordinate. From a computational point of view, such effects are practically impossible to study with direct molecular dynamics. To understand the reason, let us recall the shape of the energy landscape of a protein [a description of the modern energy landscape view of biomolecules can be found in the recent textbook of Wales[48]]. It consists of a very large number of local minima (conformations), separated by barriers whose height ranges from moderate to high. The time evolution of the system in this landscape consists of relatively long periods of oscillations in the local minima, separated by hops between conformations.

The rate-promoting vibrations we examined earlier are fluctuations within a single conformation. The problem we want to address is whether there are some conformations that favor catalysis, for example, because in them the average donor−acceptor distance is shorter. To study this problem, we would like to have our molecular dynamics trajectory visit as many conformations as possible. However, the system spends most of its time in fluctuations within a conformation local minimum and only rarely hops to a different conformation minimum (see Figure 23). Therefore, MD simulations

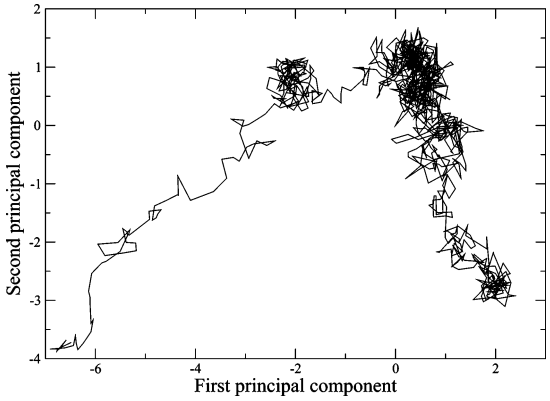

Figure 23. A 100 ps MD trajectory of PNP, plotted in the plane of the two largest principal components. The two darker regions, where the trajectory fluctuates locally, are two conformations. If we are interested in sampling many conformations, the long time the system spends in local fluctuations in a given conformation is a waste of resources.

may be useful for studying other problems, but they are not a practical tool for searching the conformation space. However, there are other techniques that may be useful. In the rest of this section, we will first briefly review recent work of other groups on conformational fluctuations that enhance reaction in dihydrofolate reductase; we will close with a computational scheme we propose for studying this class of problems.

5.1. Dihydrofolate Reductase (DHFR)

Dihydrofolate reductase (DHFR) catalyzes the reduction of 7,8-dihydrofolate (DHF) to 5,6,7,8-tetrahydrofolate (THF) through the oxidation of the coenzyme NADPH. DHFR has been studied extensively due to its role in maintaining intracellular pools of THF, which is an important component of several metabolic pathways. The reaction catalyzed by DHFR is thought to involve transfer of a proton followed by a hydride to DHF.

It has been shown through X-ray crystallography studies[49,50] that the catalytic cycle involves conformational changes of the M20 loop. This mobile loop is close to the active site and is assumed to play an important role in binding of the cofactor and substrate to DHFR. Also, mutational studies have identified distal residues[51] that affect catalysis. These studies strongly suggest that conformational changes at microsecond to nanosecond range are related to catalysis.

In addition, classical MD simulations[52] have identified correlated domain motions in the reactant DHF complex but not in product complexes, suggesting they may be related to catalysis. These domains are in the same regions highlighted by the NMR studies.

We will only present a very brief review of theoretical studies on this system and refer to reader to publications of the groups that have studied it.[53−55] Since the catalytic step involves a hydride transfer, a major difficulty is how to treat quantum effects. These works followed different paths.

Truhlar, Gao, and Garcia-Viloca[53] use a geometric reaction coordinate, the difference between acceptor-hydrogen and donor-hydrogen distances. The system is divided into a small primary zone at the active site and a secondary zone. The results are averaged over several secondary zone configurations. Electronic quantum effects are included with a semiempirical QM/MM potential that is augmented with a valence bond term, parametrized to fit the experimental free energies. The free energy profile is calculated with an umbrella sampling along the above reaction coordinate. Brooks and Thorpe[55] also used a semiempirical QM/MM potential. Only structures from the reactant side were used, and those with donor−acceptor distance smaller than 2.5 Å were used in the QM/MM calculations. For each of these configurations, a QM/MM optimization was performed for a series of fixed hydrogen acceptor distances. Only atoms within 10 Å from the transferring hydrogen were allowed to move. Hammes-Schiffer[54] used as a reaction coordinate the energy difference between reactant and product diabatic states, averaged over the ground state of the vibrational wave function of the transferred hydrogen. Electronic quantum effects are included through an EVB potential, parametrized to fit experimental free energies of activation. The free energy profile is generated by sampling over the entire range of that collective reaction coordinate. Once the energy profile is found, they used TST to calculate the reaction rate. Note that in real time the protein dynamics may need, for example, 1 ms to move along the reaction pathway of the reactive coordinate used in these works, so the generation of the energy profile allowed them to describe an event that requires time longer than any feasible molecular dynamics trajectory.

There is a long-standing debate whether approaches that calculate the free energy barrier using a geometric reaction coordinate can sufficiently sample protein conformations and whether methods that use the energy gap as the reaction coordinate are superior. In the present system, it has been

shown[53] that the two methods generate equivalent results. In fact both methods produced similar free energy profiles.

Coming back to the work of Truhlar, Gao, and co-workers[53] and Hammes-Schiffer and co-workers,[54] after they generated a free energy profile along their choice of reaction coordinate, the next step was to examine the ensemble of conformations used to generate a point on the energy profile and generate statistics and comparisons for various geometric characteristics along the energy profile. They both found a correlation of structural changes as the system approaches the transition state, which show a tightening of some hydrogen bonds and of the donor−acceptor distance.

We should emphasize that the structural changes found in those works were not motions in real time. Even if it is true that conformational changes affect catalysis, it is not clear whether the enhancement of the rate is due to a coupling to the motion of the hydride or due to different thermodynamic averages, for example, because the transfer distance became shorter. The fact that in the calculations of Brooks and Thorpe[55] most of the enzyme was held fixed is an indication that the effect is structural rather than dynamical. In this last work, a wide range of barrier heights was found, which led to questioning whether approaches that are based on mean field potentials can capture the range of protein conformations that led to that range of energy profiles. Various opinions on these questions can be found in the original papers.

To avoid semantic confusion, we should clarify that Hammes-Schiffer uses the term "promoting motion" to describe an ensemble of conformations that for example, have a shorter donor−acceptor distance. The "motion" in her case is the implied intraconversion among these conformations. The "promoting vibration" we described earlier refers to fluctuations within a single conformation. The two effects are different and occur in separate time scales.

The identification of the way conformational fluctuations in DHFR affect particular distances at the TS is a significant achievement. These simulations identified distances that change in the TS, but they cannot distinguish whether they must change in a particular order (e.g., as found with TPS in LDH). Also, they generated an ensemble of conformations near the TS, but since they have no notion of time, they cannot give details of how the system samples the conformations. In the next subsection, we will propose a scheme that may provide a starting point for a discussion that will address these questions.

5.2. Searching the Conformation Space

It would be desirable to have a more systematic method for searching for conformational fluctuations that are coupled to the reaction coordinate. In the rest of this subsection, we will propose a computational scheme that tries to address this problem. This scheme is unpublished work. It consists of three elements.

1. The topological structure of the conformation space.

2. An algorithm (string method) for calculating energetic barriers between conformations.

3. A computational scheme (kinetic Monte Carlo) for describing dynamics in the conformation space.

5.2.1. The Topological Structure of Conformation Space

It is well-known that conformations that have similar geometries have similar energies, but the opposite is not true, conformations that are unrelated may accidentally have similar energies. In addition, long MD runs that visit several conformations, sample geometrically similar conformations. The above observations suggest that conformations populate their configuration space in some structured way. The structure of the conformation space was studied by Berry,[56] Karplus and Becker,[57] and Becker.[58] They termed it "topological" structure because the key in the description is neither geometrical similarity nor energy, but rather connectivity.

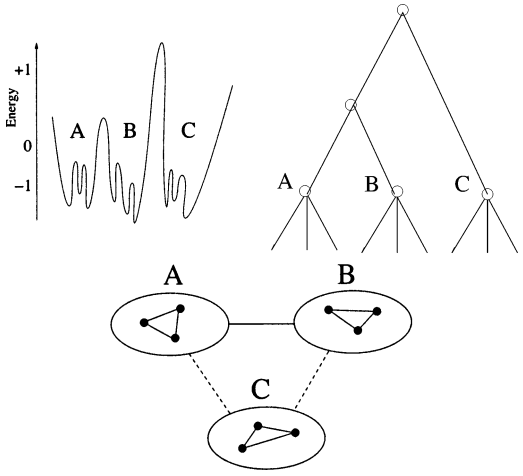

Figure 24. The topological structure of conformation space: (left) the energetic profile; (right) the connectivity graph; (bottom) the clustering of conformations into basins.

The main conclusions of this work are summarized in Figure 24. In the left panel, we see a free energy profile. At the energy level marked as "−1", any transition between conformations has to cross a saddle point. At the energy level marked as "0", the conformations that are clustered under A are accessible to each other. The same is true for the conformations under B and under C. A group of conformations, such as the ones clustered under A or B, is called a "basin". There are three basins visible in the diagram: A, B, and C. At the energy level marked as "+1", one can go from A to B, but to go from basin B to basin C, one has to cross another saddle point. We say that A and B belong to the same "superbasin", but C belongs to a different superbasin.

The above structure is depicted in the "connectivity graph" shown in the middle panel, which shows how the various conformations and saddle points are connected. An easier to understand schematic picture is shown in the right panel: the solid dots are conformations, and they are grouped in their basins. Solid lines represent transitions through a single saddle point, possible either between conformations in the same basin or between basins A and B. Basins A and B are connected to basin C by a dashed line to signify that they belong to a different superbasin and one has to cross two saddle points instead of one for a transition to C.

Becker and Karplus[57] classified in this manner all the minima and saddle points of a small peptide, met-enkephalin, and found the topological structure shown in Figure 24. It should be noted that Frauenfelder and Wolynes,[59] from their analysis of experimental data, had predicted earlier that the energy landscape of proteins would have the topological structure shown in Figure 24. In addition, they found that conformations that belong to the same basin are separated by low barriers of a few k_BT. Basins are separated from each other by a high barrier. That is, a basin consists of geometrically similar conformations that are separated by low barriers and is separated from another basin by a high

barrier. This structure explains the observations mentioned at the beginning of this subsection. A constellation of basins can have various structures,[48] one of which corresponds to the well-known "funnel" landscape of proteins.[60]

From the dynamic point of view, the protein frequently hops among conformations in the same basin, and it rarely hops to a different basin.

5.2.2. Basin Hopping in the Conformation Space

In the beginning of this section, we mentioned that even a MD trajectory that is several nanoseconds long can sample only a few conformations. With the help of the basin picture, we now realize that the conformations sampled by a MD run all lie in the same basin. The reason is that, by definition, only these conformations that are separated by low barriers, can be overcome in the time scale accessible to MD runs. A simple corollary is that the MD run would be able to sample more conformations, if it could somehow be able to hop to a neighboring basin.

Now, imagine that we have two conformations that belong to different basins and that we know the height of the barrier that separates these two conformations. Things become more interesting if we recall that the conformations that belong to the same basin are geometrically and energetically similar to each other; therefore we can pick any conformation as representative of that basin. We can make the following assumption, first suggested by Berry[56] (he recently applied it to a study of a small peptide[61]): each basin is represented by any conformation in it, and hopping among basins can be approximated by transitions among their representative conformations. In our case, one can use transition state theory to describe these transitions.

To implement the algorithm, we need a method for identifying the energetic barrier between two conformations. This is a specific case of a more general problem: given two states that lie in local minima of the energy landscape, find the minimum energy path that connects them. This is a difficult problem that has attracted a lot of activity in the past decade. Most of the algorithms used were suitable only for smooth energy landscapes. Recently, the "string" algorithm was devised for rugged landscapes and was used for finding the transition path in alanine dipeptide.[62]

This is a summary of the proposed scheme for studying dynamics in conformation space.

1. Generate many protein conformations.

2. Classify them into basins, e.g. using differences in RMSD as the criterion, and keep one representative conformation from each basin.

3. Find the energetic barriers between these representative conformations, using the string method.

4. Once a set of conformations and the rates of conversions among them has been determined, we can use a standard algorithm (e.g., kinetic Monte Carlo[63]) to describe the dynamics of hopping in the conformation space.

Note that this basin searching is much simpler than the protein folding problem, because we are only interested in conformations with energies relatively close to the native state.

What we gained compared to standard MD simulations is that the extremely long trajectories required until the system hops to a different basin have been replaced by a transition described by TST and kinetic Monte Carlo. In this way, one is able to sample many more conformations than with an ordinary MD simulation.

To connect these abstract concepts with the subject of this review paper, let us imagine that in an enzyme where a hydrogen is transferred through tunneling, there are some conformations that have donor−acceptor distance that are on average closer than other conformations. Unlike the rate-promoting vibrations we discussed earlier, whose time scale was so fast that several oscillations were needed before the proton is transferred, once the protein reaches a conformation in which donor and acceptor are close, it stays in that conformation for long enough time that tunneling takes place in that configuration of donor−acceptor. Then, conformational fluctuations that bring the protein toward these favorable for reaction conformations will strongly enhance the rate. The scheme outlined above not only can identify such favorable conformations but also can describe dynamically how they are visited by the protein.

6. References

(1) Pauling, L. *Nature* **1948**, *161*, 707.
(2) Jencks, W. *Adv. Enzymol.* **1975**, *43*, 219.
(3) Schramm, V. *Arch. Biochem. Biophys.* **2005**, *433*, 13.
(4) Wolfenden, R. *Acc. Chem. Res.* **1972**, *5*, 10.
(5) Romesberg, F.; Schowen, R. *Adv. Phys. Org. Chem.* **2004**, *39*, 27.
(6) Kohen, A. In *Biological Aspects of Hydrogen Transfer*; Schowen, R., Klinman, J., Hynes, J., Eds.; Handbook of Hydrogen, Vol. 2; Wiley: Weinheim, Germany, 2005.
(7) Masgrau, L.; Basran, J.; Hothi, P.; Sutcliffe, M.; Scrutton, N. *Arch. Biochem. Biophys.* **2004**, *428*, 41.
(8) Knapp, M. J.; Klinman, J. P. *Eur. J. Biochem.* **2002**, *269*, 3113.
(9) Bell, R. P. *The Tunnel Effect in Chemistry*; Chapman and Hall: New York, 1980.
(10) Marcus, R. A.; Sutin, N. *Biochim. Biophys. Acta* **1985**, *811*, 265.
(11) Topaler, M.; Makri, N. *J. Chem. Phys.* **1994**, *101*, 7500.
(12) Schwartz, S. D. *J. Chem. Phys.* **1996**, *105*, 6871.
(13) Hänggi, P.; Talkner, P.; Borkovec, M. *Rev. Mod. Phys.* **1990**, *62*, 251.
(14) Straub, J. E.; Borkovec, M.; Berne, B. J. *J. Phys. Chem.* **1987**, *91*, 4995.
(15) Zwanzig, R. *J. Stat. Phys.* **1973**, *9*, 215.
(16) Truhlar, D. In *Isotope Effects in Chemistry and Biology*; Kohen, A., Limbach, H., Eds.; Taylor & Francis, CRC Press: Boca Raton, FL, 2006.
(17) Borgis, D.; Hynes, J. T. In *The Enzyme Catalysis Process*; Cooper, A., Houben, J., Chien, L., Eds.; Plenum: New York, 1989.
(18) Borgis, D.; Hynes, J. T. *J. Chem. Phys.* **1991**, *94*, 3619.
(19) Benderskii, V.; Goldanskii, V.; Makarov, D. *Chem. Phys. Lett.* **1990**, *171*, 91.
(20) Benderskii, V.; Goldanskii, V.; Makarov, D. *Chem. Phys.* **1991**, *154*, 407.
(21) Benderskii, V.; Makarov, D.; Wight, C. *Adv. Chem. Phys.* **1994**, *88*, 1.
(22) Antoniou, D.; Schwartz, S. D. *J. Chem. Phys.* **1998**, *108*, 3620.
(23) Antoniou, D.; Abolfath, M. R.; Schwartz, S. D. *J. Chem. Phys.* **2004**, *121*, 6442.
(24) Miller, W. H. *Acc. Chem. Res.* **1976**, *9*, 306.
(25) van der Zwan, G.; Hynes, J. T. *J. Chem. Phys.* **1983**, *78*, 4174.
(26) Bergsma, J. P.; Gertner, B. J.; Wilson, K. R.; Hynes, J. T. *J. Chem. Phys.* **1987**, *86*, 1356.
(27) Agmon, N.; Hopfield, J. *J. Chem. Phys.* **1983**, *79*, 2042.
(28) Caratzoulas, S.; Schwartz, S. D. *J. Chem. Phys.* **2001**, *114*, 2910.
(29) Kiefer, P.; Hynes, J. *J. Phys. Chem. A* **2004**, *108*, 11793.
(30) Zavodszky, P.; Kardos, J.; Svingor, A.; Petsko, G. *Proc. Natl. Acad. Sci. U.S.A.* **1998**, *95*, 7406.
(31) Kohen, A.; Cannio, R.; Bartolucci, S.; Klinman, J. *Nature* **1999**, *399*, 496.
(32) Kohen, A.; Klinman, J. *J. Am. Chem. Soc.* **2000**, *122*, 10738.
(33) Liang, Z.; Lee, T.; Resing, K. A.; Ahn, N. G.; Klinman, J. P. *Proc. Natl. Acad. Sci. U.S.A.* **2004**, *26*, 9556.
(34) Antoniou, D.; Schwartz, S. D. *J. Phys. Chem. B* **2001**, *105*, 5553.
(35) Caratzoulas, S.; Mincer, J. S.; Schwartz, S. D. *J. Am. Chem. Soc.* **2002**, *124*, 3270.
(36) Dellago, C.; Bolhuis, P.; Csajka, F.; Chandler, D. *J. Chem. Phys.* **1998**, *108*, 1964.
(37) Dellago, C.; Chandler, D. In *Bridging the time scales: molecular simulations for the next decade*; Nielaba, P., Mareschal, M., Ciccotti, G., Eds.; Lecture Notes in Physics, Vol. 605; Springer-Verlag: New York, 2003.

(38) Basner, J. E.; Schwartz, S. D. *J. Am. Chem. Soc.* **2005**, *127*, 13822.
(39) Radhakrishnan, R.; Schlick, T. *Proc. Natl. Acad. Sci. U.S.A.* **2004**, *101*, 5970.
(40) Núñez, S.; Antoniou, D.; Schramm, V. L.; Schwartz, S. D. *J. Am. Chem. Soc.* **2004**, *126*, 15720.
(41) Lewandowicz, A.; Schramm, V. L. *Biochemistry* **2004**, *43*, 1458.
(42) Schramm, V. L. *Acc. Chem. Res.* **2003**, *36*, 588.
(43) Fedorov, A.; Shi, W.; Kicska, G.; Fedorov, E.; Tyler, P. C.; Furneaux, R. H.; Hanson, J. C.; Gainsford, G. J.; Larese, J. Z.; Schramm, V. L.; Almo, S. C. *Biochemistry* **2001**, *40*, 853.
(44) Núñez, S.; Wing, C.; Antoniou, D.; Schramm, V. L.; Schwartz, S. D. *J. Phys. Chem. A* **2006**, *110*, 463.
(45) Amadei, A.; Linssen, A. B. M.; Berendsen, H. J. C. *Proteins* **1993**, *17*, 412.
(46) de Groot, B. L.; Amadei, A.; Scheek, R. M.; van Nuland, N. A. J.; Berendsen, H. J. C. *Proteins* **1996**, *26*, 314.
(47) Erion, M. D.; Takabayashi, K.; Smith, H.; Kessi, J.; Wagner, S.; Honger, S.; Shames, S.; Ealick, S. E. *Biochemistry* **1997**, *36*, 11725.
(48) Wales, D. *Energy Landscapes: Applications to Clusters, Biomolecules and Glasses*; Cambridge University Press: Cambridge, U.K., 2003.
(49) Osborne, M.; Schnell, J.; Benkovic, S.; Dyson, H.; Wright, P. *Biochemistry* **2001**, *40*, 9846.
(50) Sawaya, M.; Kraut, J. *Biochemistry* **1997**, *36*, 586.
(51) Rajagopalan, P.; Lutz, S.; Benkovic, S. *Biochemistry* **2002**, *41*, 12618.
(52) Radkiewicz, J.; Brooks, C. L. *J. Am. Chem. Soc.* **2000**, *122*, 225.
(53) Garcia-Viloca, M.; Truhlar, D.; Gao, J. *Biochemistry* **2003**, *42*, 13558.
(54) Hammes-Schiffer, S. *Curr. Opin. Struct. Biol.* **2004**, *14*, 192.
(55) Thorpe, I.; Brooks, C. *Proteins: Struct., Funct., Bioinf.* **2004**, *57*, 444.
(56) Berry, R. S.; Kunz, R. *Phys. Rev. Lett.* **1995**, *20*, 3951.
(57) Becker, O.; Karplus, M. *J. Chem. Phys.* **1997**, *106*, 1495.
(58) Becker, O. *Proteins: Struct., Funct., Genet.* **1997**, *27*, 213.
(59) Frauenfelder, H.; Sligar, S.; Wolynes, P. *Science* **1991**, *254*, 1598.
(60) Wolynes, P. *Philos. Trans. R. Soc. London, Ser. A* **2005**, *363*, 453.
(61) Despa, F.; Fernandez, A.; Berry, R. S.; Levy, Y.; Jortner, J. *J. Chem. Phys.* **2003**, *118*, 5673.
(62) Ren, W.; Vanden-Eijnden, E.; E, W. *J. Chem. Phys.* **2005**, *123*, 134109.
(63) Fichthorn, K.; Weinberg, W. *J. Chem. Phys.* **1991**, *95*, 1090.

CR0503052